THE JOURNAL OF PHYSICAL CHEMISTRY Letters

pubs.acs.org/JPCL Letter

New Pressure Stabilization Structure in Two-Dimensional $PtSe_2$

Kai Jiang,[⊥] Anyang Cui,[⊥] Sen Shao,[⊥] Jiajia Feng, Hongliang Dong, Bin Chen, Yanchao Wang,* Zhigao Hu,* and Junhao Chu

HPSTAR 1000-2020

Cite This: J. Phys. Chem. Lett. 2020, 11, 7342−7349 Read Online

ACCESS | Metrics & More | Article Recommendations

ABSTRACT: The frequency shifts and lattice dynamics to unveil the vibrational properties of platinum diselenide ($PtSe_2$) are investigated using pressure-dependent polarized Raman scattering at room temperature up to 25 GPa. The two phonon modes E_g and A_{1g} display similar hardening trends; both the Raman peak positions and full widths at half-maximum have distinct mutation phenomena under high pressure. Especially, the split E_g mode at 4.3 GPa confirms the change of the lattice symmetry. With the aid of the first-principles calculations, a new pressure stabilization structure *C*2/*m* of $PtSe_2$ has been found to be in good agreement with experiments. The band structures calculations reveal that the new phase is a novel type-I Dirac semimetal. The results demonstrate that the pressure-dependent Raman spectra combined with theoretical predictions may open a new window for searching and controlling the phase structure and Dirac cones of two-dimensional materials.

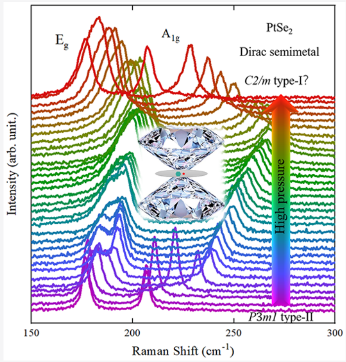

Recently, layered transition metal dichalcogenides (TMDs) have been in the spotlight of the research community because of their physical properties and promising potential applications in the field of electronics and optoelectronics.[1−6] Platinum diselenide ($PtSe_2$) has emerged as an interesting compound that belongs to TMDs and predicted the highest phonon limited electron mobility among the previous studied TMDs materials at room temperature.[7,8] In particular, $PtSe_2$ has proved to be an attractive candidate for a variety of applications due to its unique electronic property whereby theoretical studies proposed a transition from semimetal to semiconductor by controlling the layer numbers.[9−11] Recently, both theoretical predictions and experimental results have confirmed that bulk 1T-$PtSe_2$ is a novel type-II Dirac semimetal.[12−16] Previous study has shown that the type-II Dirac Fermions protected by C_3 rotational symmetry about the *c* axis can exist in the $PtSe_2$ family of materials.[13] Following the predictions, evidence of type-II Dirac cones in $PtSe_2$ was soon characterized in quantum oscillations, angle-resolved photoemission spectroscopy and negative longitudinal magnetoresistance by different groups.[14,17−19] Investigating such topological phase transitions in Dirac semimetal materials not only offers unique opportunities for studying the fundamental properties of Fermions but also holds potential for device applications exploiting their exotic surface excitations and bulk electric, optical and vibrational properties.[15]

It is well-known that the application of high pressure by modifying the lattice structure can be an effective tool to tune the structure and physical properties of $PtSe_2$.[20,21] The phase transitions, chemical reaction, and anharmonicity in the lattice potential energy can be found because of the atomic and electronic arrangements under extreme conditions.[22−25] Furthermore, the band structures are related to their Dirac cones, which are sensitive to the out-of-plane and in-plane interactions. Although there are reports of high-pressure behavior of phonons in $PtSe_2$ on crystals using Raman spectroscopy,[26−31] the phonon behaviors of $PtSe_2$ at Dirac point under proper pressure are not known. Previous work in $PtSe_2$ has concentrated on X-ray diffraction studies from pressure-induced phase transitions. However, they have not found the structure transition up to 30 GPa according to the results from X-ray diffraction and electrical transport.[28,32] Therefore, the knowledge of the $PtSe_2$ structural stability range under conditions of variable pressures is important for such applications.

In this Letter, we establish the pressure phase diagram of the Dirac semimetal $PtSe_2$ by high-pressure Raman scattering and theoretical calculations. Both the E_g and A_{1g} Raman modes display anomalies in the phonon frequencies accompanied by abnormal evolution of their line width starting at ∼4.3 GPa. The theoretical prediction indicates that the pressure can induce the appearance of type-I Dirac cones. The phonon spectra and band structure of $PtSe_2$ are investigated under

Received: June 12, 2020
Accepted: August 12, 2020
Published: August 12, 2020

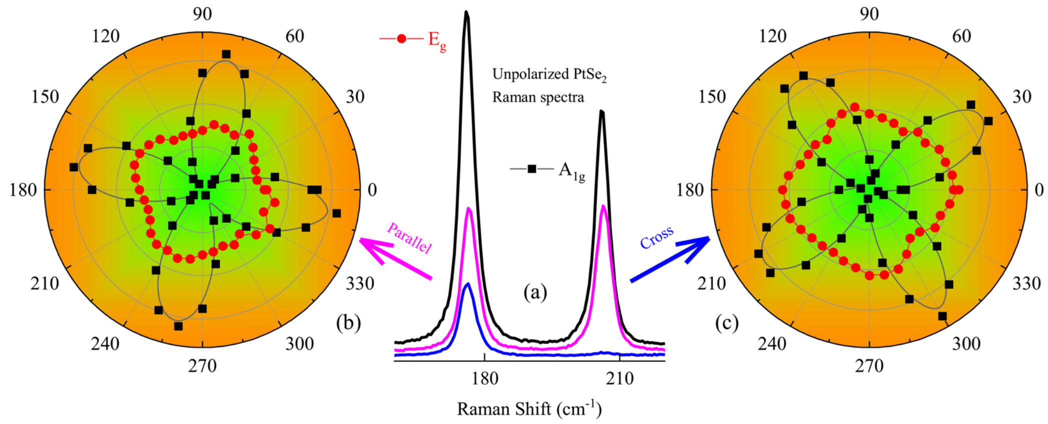

Figure 1. (a) Polarized Raman spectra of $PtSe_2$ single crystal measured at ambient conditions. (b) and (c) Summarized intensity of the E_g and A_{1g} modes as a function of the polarization of incidence light for parallel (red line) and cross (blue line) $PtSe_2$.

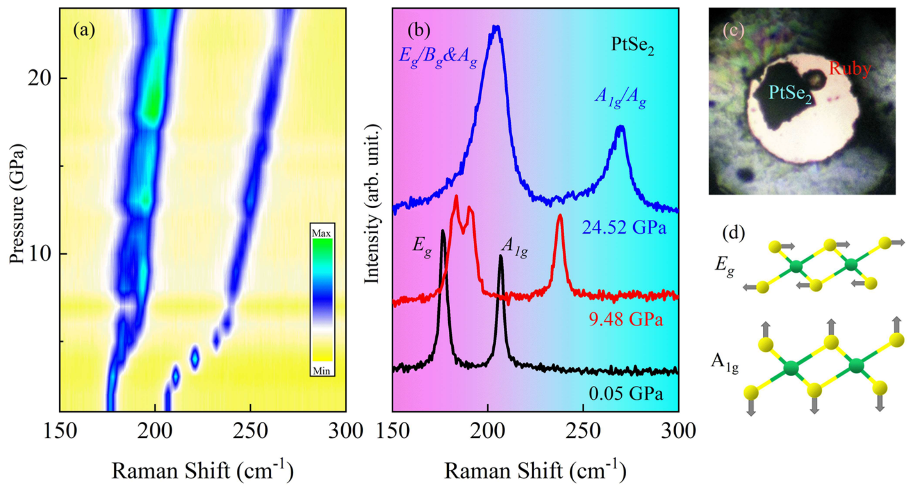

Figure 2. (a) Pressure maps of Raman scattering and (b) selected Raman spectra for $PtSe_2$ from ambient up to 25 GPa at room temperature. Note that each spectrum is shifted in intensity for clarity. (c) Top view of the $PtSe_2$ sample and ruby in a diamond anvil cell. (d) Schematic views of two Raman-active vibrational modes in $PtSe_2$.

different pressures. We unambiguously determine a new pressure stabilization structure and underlying structural mechanisms of the transitions up to 25 GPa. The observation of the transition in 1T-$PtSe_2$ under high pressure provides an engineering approach to optimizing the phase as needed in applications, which not only opens up a new window for searching and controlling the phase structure and Dirac cones of the other two-dimensional materials but also promotes the practical development of reversing activity related materials and devices.[33]

Polarized Raman spectra measurements of the $PtSe_2$ single crystal (from 2D semiconductors) were carried out using a Jobin-Yvon LabRAM HR Evolution spectrometer (Figure 1). The sample was loaded in a Mao-Bell type diamond anvil cell (DAC) with a 300 μm culet diamond and a stainless steel gasket (Figure 2). As we know, the Raman spectra of $PtSe_2$ have higher sensitivity with the different thickness like the other two-dimensional materials.[1,10,26,29,30] The thickness of $PtSe_2$ is about 10 μm in our DAC for the high-pressure Raman experiment. The thickness of the $PtSe_2$ material will not change under the action of hydrostatic pressure. Thus, we can exclude the effect of thickness on our Raman spectra. Silicon oil was used as the pressure transmitting media, which maintains hydrostatic conditions up to 30 GPa. In all high-pressure experiments, the R1-line emission of a tiny ruby was used for pressure calibration.[34] The polarized Raman spectra were recorded in backscattering geometry in parallel and perpendicular polarization configurations. Raman spectra were obtained by excitation with a 532 nm Nd:YAG laser beam and a 1800 grooves/mm grating. The laser beams were focused on the sample by a ×50 objective with a working distance of 18 mm. The laser was focused to a 2 μm spot with incident power on the DAC limited below 1 mW before the sample in order to reduce the laser heating effect on the surface.

The structure searching is performed by the swarm-intelligence based CALYPSO method as implemented in its same-name CALYPSO code,[35−37] which is based on a global minimization of free energy surfaces merging ab initio total-energy calculations. We searched for the structures of $PtSe_2$ with simulation cell sizes ranging from 1 to 4 formula units at 10 and 20 GPa, respectively. And due to the massive computational cost of predicting structures for large formula unit of $PtSe_2$, a high-throughput screening of AB_2 type materials (up to 32 f.u.) is also performed on the basis of the Material Project.[38]

Structure optimizations and electronic calculations are performed in the framework of density functional theory[39] within the generalized gradient approximation[40] as imple-

https://dx.doi.org/10.1021/acs.jpclett.0c01813
J. Phys. Chem. Lett. 2020, 11, 7342−7349

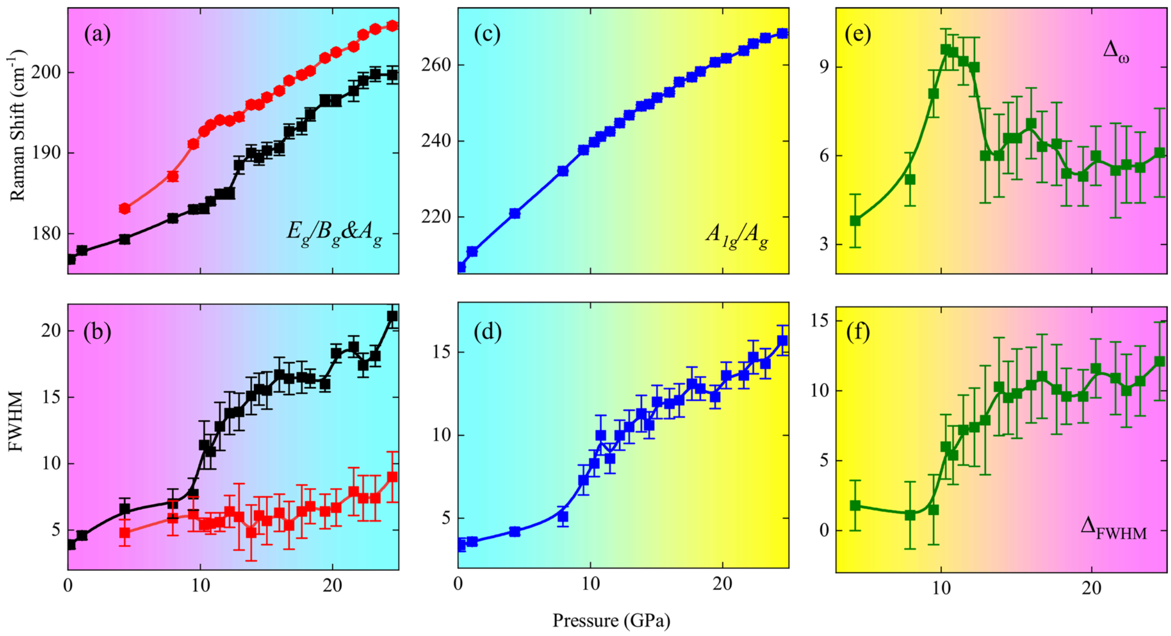

Figure 3. Pressure dependence of the (a), (b) E_g/B_g and A_g and (c), (d) A_{1g}/A_g Raman phonon modes from ambient pressure to 25 GPa as determined from the data of Figure 2. (e), (g) Difference of the Raman shift and fwhm for the split E_g/B_g and A_g mode, showing the phase transition regions.

mented in the VASP code.[41] The all-electron projector-augmented wave (PAW) method[42] is adopted with $5d^96s^1$ and $4s^24p^4$ configurations treated as the valence electrons of Pt and Se, respectively. A kinetic cutoff energy of 600 eV and the spacing of 0.2 for Monkhorst−Pack k-mesh sampling were adopted in order to ensure the enthalpy calculations converged within 1 meV/atom. The van der Waals density-functional approach (vdW-DF) with the optB86b function[43] is adopted in our calculations. The dynamic stability of the new structures is verified from phonon calculation using the finite displacement method as implemented in PHONOPY code.[44] The calculation of Raman spectrum was performed in the vaspraman.py package with the VASP code as a back-end.

The optimized atomic structure of the octahedral coordination forming the 1T polytype of $PtSe_2$ belongs to $P\bar{3}m1$ space group. For the primitive unit cell of 1T-$PtSe_2$ composed of three atoms, the phonon spectra includes nine phonons, i.e., three acoustic and six optical branches. According to the lattice dynamics analysis, the decomposition of the vibration representation of optical modes at the Γ point is $\Gamma = 2E_g + 2E_u + A_{1g} + A_{2u}$ for the 1T-$PtSe_2$ structure. Optical phonon modes include two doubly degenerate in-plane vibration modes, the Raman-active E_g mode and the infrared-active E_u mode, and two single degenerate out-of-plane vibrational modes, the Raman-active A_{1g} mode and the infrared-active E_{2u} mode.

As shown in Figure 1a, the two Raman peaks E_g and A_{1g} can be observed in the experiments. The E_g mode located at ∼176.3 cm^{-1} corresponds to an intralayer in-plane vibration of Se atoms moving in opposite directions. The A_{1g} mode located at ∼206.7 cm^{-1} involves the out-of-plane vibration of Se atoms moving away from each other. The details of the schematic diagram of the two modes are shown in Figure 2d. The intensity of the E_g mode is higher than that of A_{1g} mode. This indicates that the *c*-axis motion of Se atoms has less contribution in the Raman intensity compared to the *a*−*b* plane motion of the Se atoms according to the strong covalent character between Pt and Se atoms. Figure 1 also shows the differences in the polarized and unpolarized Raman spectra of the $PtSe_2$ single crystal. All of the phonon modes are visible in the unpolarized or parallel polarization measurement, whereas in a crossed polarization Raman spectra the higher energy A_{1g} mode is vanished. Therefore, we believed that the A_{1g} mode is sensitive to polarization analysis. Figure 1b,c show the intensities of the two Raman phonon modes in polar axis. The intensity of the A_{1g} mode is polarization dependent, while the E_g mode is independent with increasing angle from 0° to 360°. According to the Raman polarization-dependent tensors, the polarization dependence of the scattering intensity expressed as $I_s(E_g) \propto d^2$ and $I_s(A_{1g}) \propto a^2(\cos\varphi)^2$, where φ is the polarization angle of the incident light.[30,45] From the theoretical and polarization Raman spectra results, we confirmed the in-plane mode as E_g with polarization independence, and the out-of-plane mode as A_{1g} with polarization dependence, respectively. Note that the polarized Raman spectra show a 4-fold symmetry rather than a 2-fold symmetry such as PtS_2.[4,30] For the A_{1g} mode under the parallel configurations, the maximum peak intensities occur at 80°, 170°, 260°, and 350° while the minimum intensities occur at 30°, 120°, 210°, and 300°. The Raman peaks under cross configurations show the opposite trend, as shown in Figure 1c. This phenomenon indicates that the peak intensities of the Raman mode are related not only to the polarization incident light angle but also to the parallel and cross configurations during the scattered lights. The highly Raman anisotropy in $PtSe_2$ enables us to investigate its physical properties as a polarization sensitive photodetector.

Parts a and b of Figure 2 display the normalized Raman spectral maps and a series of Raman spectra with selected pressures during the compression procedures. Consistent with previous reports, the two Raman phonon modes exhibit blue shifts with increasing pressure up to 25 GPa, and their intensities also simultaneously decrease. The pressure coefficients for the two modes are clearly different, especially for

Table 1. Detailed Lattice Structure of $PtSe_2$ with Different Symmetries

			atomic coordinates (fractional)		
space group	lattice parameters (Å)	atoms	*X*	*Y*	*Z*
$P\bar{3}m1$	$a = b = 3.78300$	Pt(1b)	0.00000	0.00000	0.50000
	$c = 4.98560$	Se(2d)	0.33333	0.66667	0.75936
	$\gamma = 120.00$	$\alpha = \beta = 90.00$			
$C2/m$	$a = 6.54610$n $b = 3.78220$	Pt(2a)	0.50000	0.50000	0.00000
	$c = 5.00470$	Se(4i)	0.83321	0.50000	0.74133
	$\beta = 90.05$	$\alpha = \gamma = 90.00$			

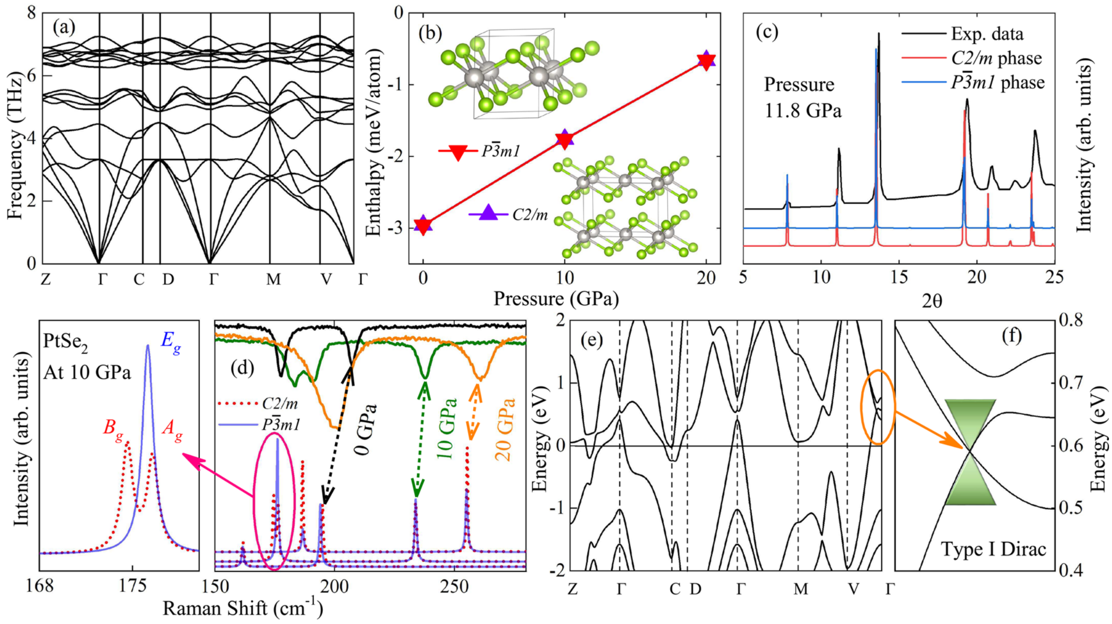

Figure 4. (a) Phonon spectra of the pressure stabilization structure $C2/m$ of $PtSe_2$ at 10 GPa. (b) Calculated static energies of $PtSe_2$ with different space groups under pressure. The insets illustrate oblique view of the crystal structure of $PtSe_2$ with the $P\bar{3}m1$ and $C2/m$ phases. Green balls are Se atoms, and gray balls are Pt atoms. (c) Experimental and calculated XRD results of $PtSe_2$ at high pressure. (d) Experimental (upper) and calculated (lower) Raman spectra under different pressures for the $PtSe_2$ single crystal. The solid lines are the $P\bar{3}m1$ phase and the dotted lines are the $C2/m$ phase. The picture on the left is an enlarged view of the E_g mode in the $P\bar{3}m1$ phase and B_g and A_g modes in the $C2/m$ phase at 10 GPa. (e) Band structure of $PtSe_2$ under 10 GPa. (f) Schematic diagram of the type-I Dirac cone in the enlarged $PtSe_2$ band structure under high pressure.

the A_{1g} mode below 10 GPa with an abrupt anomaly. Note that the A_{1g} mode is very sensitive to the pressure in the low-pressure region, which may link to its high mechanical property and sensor. The different sensitivity mechanism of the phonon mode can be attributed to the different changes between the interlayer distance and interatomic distance with increasing pressure. The interlayer distance decreases from 2.40 to 2.00 Å in the low-pressure range, 16.45% reduction in percentage. However, the value of the percentage is only 7.68% in the high pressure range. Moreover, the peak intensity of the E_g mode relative to that of the A_{1g} mode increases with pressure, consistent with the changes of vdW interactions in $PtSe_2$ single crystal. Interestingly, the two modes show a different scenario. The E_g mode splits into two peaks at ~183 and ~191 cm^{-1} in Figure 2b. As we know, the split Raman peak indicates the change of the lattice symmetry in $PtSe_2$. With increasing pressure, the split two peaks have a blue shift and merge into one broader peak. The anomalous behavior can be attributed to pressure-induced structural changes and long-range Coulombic interlayer interactions.[31] The observation of the split double peak at low-frequency zone corresponding to E_g Raman mode region of $P\bar{3}m1$ space group suggests that there may be some changes in structure or phase. It is unknown whether the split Raman peak still belong to the E_g mode of $P\bar{3}m1$ or not. We will predict the structures of $PtSe_2$ at high pressure using CALYPSO method and its same-name code in the discussion of the following letter. There are significant changes between the *c*-axis and interlayer distance of $PtSe_2$ single crystal with increasing the pressure according to our calculation from ambient pressure to 20 GPa. The interlayer distance is reduced by 22.1% from 2.40 to 1.87 Å with the high pressure. The bond length between Pt and Se atoms also decreases from 2.54 to 2.47 Å, only about 2.8% variations. Therefore, the pressure induced interlayer mechanical interaction is highly anisotropic for A_{1g} mode, which is consist with the polarization Raman spectra results.

The Lorentz function is used to analyze the details vibration properties of the two modes, as presented in Figure 3. The pressure induced evolutions of E_g and A_{1g} modes are reversible, and the resulting blue shifts with pressure from 0 to 25 GPa are 23 and 62 cm^{-1}, respectively. The continuous blue shifts of both peaks indicate the strengthened interaction between Pt and Se atoms caused by the contraction of the lattice under high pressure. The out-of-plane vibration A_{1g} changes the strength of interlayer mechanical coupling by decreasing/increasing the interlayer distance. However, the in-plane

https://dx.doi.org/10.1021/acs.jpclett.0c01813
J. Phys. Chem. Lett. 2020, 11, 7342−7349

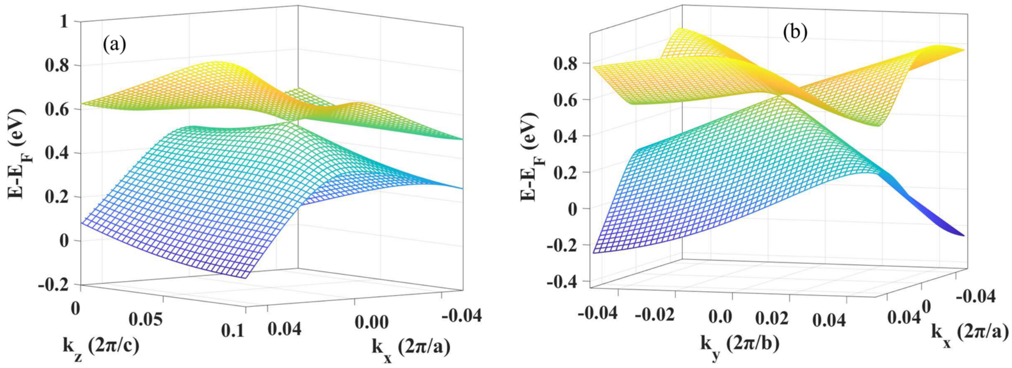

Figure 5. Three-dimensional band structures on the (a) $k_y = 0$ and (b) $k_z = 0.06$ plane around the Dirac point. The linear band crossing along three independent directions near the Dirac point confirms the type-I Dirac cone in the bulk single crystal of $PtSe_2$ under high pressure.

motion E_g only induces slight tilting of the springs, which can be driven by a much smaller force gradient.

In Figure 3, two regions corresponding to different Raman spectra can be immediately identified according to the analysis of the peak position, from ambient pressure to 10 GPa and 10−25 GPa. In the low-pressure region below 5 GPa, the E_g and A_{1g} modes are detected corresponding to the 1T phase, as confirmed in the polarization measurements. The E_g mode becomes even broader on the application of pressure and splits into two peaks above 5 GPa. The differences between the split E_g mode during compression procedures are displayed in Figure 3e,f. Furthermore, it was observed that the full width half-maximum (fwhm) increases with increasing the pressure. The E_g mode broadens from 4 cm^{-1} to above 21 cm^{-1}, while the A_{1g} mode broadens from 3 to 15 cm^{-1}. The calculated pressure coefficients $d_{\omega}(A_{1g})/d_P$ are 3.5 and 2.4 cm^{-1} GPa^{-1} for the pressure below and above 5 GPa, respectively. Both the Raman peak positions and fwhm have distinct mutation phenomena between 5 and 10 GPa, which confirms the change of the lattice under the high pressure. In many other compounds, both topological quantum phase transition and Lifshitz transition can be identified by the indirect experimental results according to the anomalies Raman shifts, intensity, and fwhm under high pressure.[21−23,31] Upon decompression, the Raman spectral changes were partially reversible immediately and the high-pressure mixed phase fully reverted to the original structure. Therefore, according to the splitting E_g peaks and distinct mutation phenomena, a structure transition can occur by pressure and lattice distortion, resulting in a change of the point group symmetry.

As noted above, the pressure-induced the change of Raman spectra demonstrates the advent of a high-pressure phase. In order to determine the structure of new phase, theoretical structure searching using CALYPSO and high-throughput screening are performed. A new pressure stabilization structure with $C2/m$ symmetry is found, whose geometry is similar to that of 1T phase containing the $PtSe_2$ layers. The detailed lattice structure parameters and schematic diagrams of $PtSe_2$ with different symmetry are shown in Table 1 and Figure 4, respectively. In order to determine the dynamic stability, the phonon spectra of new predicted structure are also calculated, depicted in Figure 4a. The absence of any imaginary phonon frequencies in the whole Brillouin zone demonstrates that the $C2/m$ phase is dynamically stable. Just as shown in Figure 4b, the differences of enthalpy for $C2/m$ and $P\bar{3}m1$ space groups are less than 1 meV/atom under pressures ranging from 0 to 20 GPa, revealing that the $C2/m$ phase may coexist with 1T phase. The comparison of XRD patterns between the theoretical simulations of $C2/m$ and $P\bar{3}m1$ space groups and experimental data at 11.8 GPa [ref 28] are presented in Figure 4c. It is evident that the difference between the $P\bar{3}m1$ and $C2/m$ structures is negligible.

In order to further confirm our prediction, we therefore calculated the Raman spectra of $C2/m$ and $P\bar{3}m1$ space groups by considering the effects of both high pressure and vdW. There are three Raman active modes B_g + $2A_g$ in the $C2/m$ phase. As shown in Figure 4d, the B_g and A_g Raman modes of $C2/m$ are degenerate and overlapped with the E_g Raman mode of $P\bar{3}m1$ in ambient conditions. However, the B_g and A_g Raman modes of $C2/m$ are split at pressures above 5 GPa, which has a good coincidence with the experimental results. In addition, they have a trend to degenerate again as the pressure increases beyond 15 GPa, which is also observed in the experiment. However, the E_g Raman mode in the $P\bar{3}m1$ phase is always degenerate in the experimental pressure range. The observation of split double peaks of the E_g mode in our experiment indicates the appearance of a new phase. The split double peaks are considered to be the B_g and A_g Raman modes of the $C2/m$ phase. As shown in Figure 3e, the difference between the low-frequency Raman mode increases during compression procedures, reaching the maximum at 10 GPa. The phase transition process is gradual rather than abrupt with increasing pressure. Then the difference decreases with increasing pressure, which leads to the observation of a large broadening peak in the low-frequency zone in the experiment. The B_g and B_g Raman modes of $C2/m$ are indiscernible and degenerate into one peak again at 15 GPa from the theoretical simulation. Note that the energetical degeneracy of $C2/m$ and $P\bar{3}m1$ as well as the E_g Raman modes of $P\bar{3}m1$ always overlapped with at least one of the B_g and A_g Raman modes of $C2/m$ in Figure 4d. Considering the results from the Raman spectrum and energetic degeneracy, it can be concluded that $C2/m$ and $P\bar{3}m1$ phases can coexist under pressure.

In order to study electronic properties, we investigate band structures with the correction of spin−orbit coupling (SOC) for the new predicted $C2/m$ phase under pressures Figure 4e. This type of material is a well-known Dirac semimetal with outstanding properties and the 1T phase of $PtSe_2$ is type-II Dirac semimetal, having been studied widely.[13,19] New predicted $C2/m$ $PtSe_2$ shows a metallic property. Along the V−Γ direction, a type-II Dirac band crossing appears within valence bands at about 1.30 eV below the Fermi energy for $C2/m$ $PtSe_2$ under 0 GPa, while a type-I Dirac point connecting the valence and conduction bands is found to

https://dx.doi.org/10.1021/acs.jpclett.0c01813
J. Phys. Chem. Lett. 2020, 11, 7342−7349

reside at about 0.5 eV above the Fermi energy under 10 and 20 GPa in Figure 4f. Type-I Dirac cone should have opposite slop sign and type-II Dirac cone should have the same slope sign. In order to confirm the new type-I Dirac cone in the bulk $PtSe_2$ single crystal,[13] the three-dimensional band structures of the $C2/m$ phase on the $k_y = 0$ and $k_z = 0.06$ planes around the Dirac point have been also investigated in Figure 5a,b, respectively. It shows the linear band crossing along all the independent directions near the Dirac point in k-space. Therefore, we concluded that the high-pressure $C2/m$ phase of $PtSe_2$ is a topological material with a type-I Dirac cone according to the calculated band structures along the three orthogonal directions from the touching point.

To summarize, we have systematically investigated the pressure dependent on structural and vibrational properties of 1T-$PtSe_2$ by Raman scattering spectroscopy and first-principles calculations. The new pressure stabilization structure $C2/m$ is found by the theoretical prediction. The structure can be also confirmed by the anomalies in the fwhm and frequencies of Raman modes with pressure and the phonon calculation results. The type-I Dirac Fermions are found according to our band structure investigations under compression, which is associated with the emergence of the new pressure stabilization structures. The results will pave the way for detecting the phase structure of TMDs under the extreme conditions.

■ AUTHOR INFORMATION

Corresponding Authors

Yanchao Wang − *State Key Laboratory of Superhard Materials & International Center for Computational Method and Software, Jilin University, Changchun 130012, China;* orcid.org/0000-0003-4518-925X; Phone: +86-21-54345150; Email: wyc@calypso.cn; Fax: +86-21-54342933

Zhigao Hu − *Technical Center for Multifunctional Magneto-Optical Spectroscopy (Shanghai), Engineering Research Center of Nanophotonics & Advanced Instrument (Ministry of Education), Department of Materials, School of Physics and Electronic Science, East China Normal University, Shanghai 200241, China; Collaborative Innovation Center of Extreme Optics, Shanxi University, Taiyuan, Shanxi 030006, China; Shanghai Institute of Intelligent Electronics & Systems, Fudan University, Shanghai 200433, China;* orcid.org/0000-0003-0575-2191; Phone: +86-21-54345150; Email: zghu@ee.ecnu.edu.cn; Fax: +86-21-54342933

Authors

Kai Jiang − *Technical Center for Multifunctional Magneto-Optical Spectroscopy (Shanghai), Engineering Research Center of Nanophotonics & Advanced Instrument (Ministry of Education), Department of Materials, School of Physics and Electronic Science, East China Normal University, Shanghai 200241, China*

Anyang Cui − *Technical Center for Multifunctional Magneto-Optical Spectroscopy (Shanghai), Engineering Research Center of Nanophotonics & Advanced Instrument (Ministry of Education), Department of Materials, School of Physics and Electronic Science, East China Normal University, Shanghai 200241, China*

Sen Shao − *State Key Laboratory of Superhard Materials & International Center for Computational Method and Software, Jilin University, Changchun 130012, China*

Jiajia Feng − *Center for High Pressure Science and Technology Advanced Research, Shanghai 201203, China*

Hongliang Dong − *Center for High Pressure Science and Technology Advanced Research, Shanghai 201203, China*

Bin Chen − *Center for High Pressure Science and Technology Advanced Research, Shanghai 201203, China*

Junhao Chu − *Technical Center for Multifunctional Magneto-Optical Spectroscopy (Shanghai), Engineering Research Center of Nanophotonics & Advanced Instrument (Ministry of Education), Department of Materials, School of Physics and Electronic Science, East China Normal University, Shanghai 200241, China; Collaborative Innovation Center of Extreme Optics, Shanxi University, Taiyuan, Shanxi 030006, China; Shanghai Institute of Intelligent Electronics & Systems, Fudan University, Shanghai 200433, China*

Complete contact information is available at:
https://pubs.acs.org/10.1021/acs.jpclett.0c01813

Author Contributions

⊥K. Jiang, A. Cui, and S. Shao contributed equally to this work. The manuscript was written through contributions of all authors. All authors have given approval to the final version of the manuscript.

Notes

The authors declare no competing financial interest.

■ ACKNOWLEDGMENTS

This work was financially supported by the National Natural Science Foundation of China (Grants Nos. 91833303, 61974043, 61805081, 61674057, 11822404, and 11774127), the National Key Research and Development Program of China (Grants No. 2018YFB0406500, 2017YFA0303403, and 2019YFB2203400), Projects of Science and Technology Commission of Shanghai Municipality (Grant Nos. 18JC1412400, 18YF1407000, 18YF1407200, and 19511120100), China Postdoctoral Science Foundation (2020TQ0099), and the Program for Professor of Special Appointment (Eastern Scholar) at Shanghai Institutions of Higher Learning.

■ REFERENCES

(1) Yu, X.; Yu, P.; Wu, D.; Singh, B.; Zeng, Q.; Lin, H.; Zhou, W.; Lin, J.; Suenaga, K.; Liu, Z.; Wang, Q. J. Atomically thin noble metal dichalcogenide: a broadband mid-infrared semiconductor. *Nat. Commun.* **2018**, *9*, 1545.

(2) Avsar, A.; Ciarrocchi, A.; Pizzochero, M.; Unuchek, D.; Yazyev, O. V.; Kis, A. Defect induced, layer-modulated magnetism in ultrathin metallic $PtSe_2$. *Nat. Nanotechnol.* **2019**, *14*, 674−678.

(3) Okogbue, E.; Han, S. S.; Ko, T.-J.; Chung, H.-S.; Ma, J.; Shawkat, M. S.; Kim, J. H.; Kim, J. H.; Ji, E.; Oh, K. H.; Zhai, L.; Lee, G.-H.; Jung, Y. Multifunctional Two-Dimensional $PtSe_2$-Layer Kirigami Conductors with 2000% Stretchability and Metallic-to-Semiconducting Tunability. *Nano Lett.* **2019**, *19*, 7598−7607.

(4) Liang, Q.; Wang, Q.; Zhang, Q.; Wei, J.; Lim, S. X.; Zhu, R.; Hu, J.; Wei, W.; Lee, C.; Sow, C.; Zhang, W.; Wee, A. T. S. High-Performance, Room Temperature, Ultra-Broadband Photodetectors Based on Air-Stable $PdSe_2$. *Adv. Mater.* **2019**, *31*, 1807609.

(5) Noh, H.-J.; Jeong, J.; Cho, E.-J.; Kim, K.; Min, B. I.; Park, B.-G. Experimental Realization of Type-II Dirac Fermions in a $PdTe_2$ Superconductor. *Phys. Rev. Lett.* **2017**, *119*, No. 016401.

(6) Wang, Z.; Li, Q.; Besenbacher, F.; Dong, M. Facile Synthesis of Single Crystal $PtSe_2$ Nanosheets for Nanoscale Electronics. *Adv. Mater.* **2016**, *28*, 10224−10229.

(7) Huang, Z.; Zhang, W.; Zhang, W. Computational Search for Two-Dimensional MX_2 Semiconductors with Possible High Electron Mobility at Room Temperature. *Materials* **2016**, *9*, 716.

(8) Wagner, S.; Yim, C.; McEvoy, N.; Kataria, S.; Yokaribas, V.; Kuc, A.; Pindl, S.; Fritzen, C.-P.; Heine, T.; Duesberg, G. S.; Lemme, M. C. Highly Sensitive Electromechanical Piezoresistive Pressure Sensors Based on Large-Area Layered $PtSe_2$ Films. *Nano Lett.* **2018**, *18*, 3738−3745.

(9) Kandemir, A.; Akbali, B.; Kahraman, Z.; Badalov, S. V.; Ozcan, M.; Iyikanat, F.; Sahin, H. Structural, electronic and phononic properties of $PtSe_2$: from monolayer to bulk. *Semicond. Sci. Technol.* **2018**, *33*, No. 085002.

(10) Yim, C.; McEvoy, N.; Riazimehr, S.; Schneider, D. S.; Gity, F.; Monaghan, S.; Hurley, P. K.; Lemme, M. C.; Duesberg, G. S. Wide Spectral Photoresponse of Layered Platinum Diselenide-Based Photodiodes. *Nano Lett.* **2018**, *18*, 1794−1800.

(11) Hu, D.; Zhao, T.; Ping, X.; Zheng, H.; Xing, L.; Liu, X.; Zheng, J.; Sun, L.; Gu, L.; Tao, C.; Wang, D.; Jiao, L. Unveiling the Layer-Dependent Catalytic Activity of $PtSe_2$ Atomic Crystals for the Hydrogen Evolution Reaction. *Angew. Chem., Int. Ed.* **2019**, *58*, 6977−6981.

(12) Wang, Y.; Li, L.; Yao, W.; Song, S.; Sun, J. T.; Pan, J.; Ren, X.; Li, C.; Okunishi, E.; Wang, Y.-Q.; Wang, E.; Shao, Y.; Zhang, Y. Y.; Yang, H.-t.; Schwier, E. F.; Iwasawa, H.; Shimada, K.; Taniguchi, M.; Cheng, Z.; Zhou, S.; Du, S.; Pennycook, S. J.; Pantelides, S. T.; Gao, H.-J. Monolayer $PtSe_2$, a New Semiconducting Transition-Metal-Dichalcogenide, Epitaxially Grown by Direct Selenization of Pt. *Nano Lett.* **2015**, *15*, 4013−4018.

(13) Huang, H.; Zhou, S.; Duan, W. Type-II Dirac fermions in the $PtSe_2$ class of transition metal dichalcogenides. *Phys. Rev. B: Condens. Matter Mater. Phys.* **2016**, *94*, 121117.

(14) Zhang, K.; Yan, M.; Zhang, H.; Huang, H.; Arita, M.; Sun, Z.; Duan, W.; Wu, Y.; Zhou, S. Experimental evidence for type-II Dirac semimetal in $PtSe_2$. *Phys. Rev. B: Condens. Matter Mater. Phys.* **2017**, *96*, 125102.

(15) Bahramy, M. S.; Clark, O. J.; Yang, B. J.; Feng, J.; Bawden, L.; Riley, J. M.; Marković, I.; Mazzola, F.; Sunko, V.; Biswas, D.; Cooil, S. P.; Jorge, M.; Wells, J. W.; Leandersson, M.; Balasubramanian, T.; Fujii, J.; Vobornik, I.; Rault, J. E.; Kim, T. K.; Hoesch, M.; Okawa, K.; Asakawa, M.; Sasagawa, T.; Eknapakul, T.; Meevasana, W.; King, P. D. C. Ubiquitous formation of bulk Dirac cones and topological surface states from a single orbital manifold in transition-metal dichalcogenides. *Nat. Mater.* **2018**, *17*, 21.

(16) Li, Y.; Xia, Y.; Ekahana, S. A.; Kumar, N.; Jiang, J.; Yang, L.; Chen, C.; Liu, C.; Yan, B.; Felser, C.; Li, G.; Liu, Z.; Chen, Y. Topological origin of the type-II Dirac fermions in $PtSe_2$. *Phys. Rev. Mater.* **2017**, *1*, No. 074202.

(17) Xiao, R. C.; Gong, P. L.; Wu, Q. S.; Lu, W. J.; Wei, M. J.; Li, J. Y.; Lv, H. Y.; Luo, X.; Tong, P.; Zhu, X. B.; Sun, Y. P. Manipulation of type-I and type-II Dirac points in $PdTe_2$ superconductor by external pressure. *Phys. Rev. B: Condens. Matter Mater. Phys.* **2017**, *96*, No. 075101.

(18) Yang, H.; Schmidt, M.; Süss, V.; Chan, M.; Balakirev, F. F.; McDonald, R. D.; Parkin, S. S. P.; Felser, C.; Yan, B.; Moll, P. J. W. Quantum oscillations in the type-II Dirac semi-metal candidate $PtSe_2$. *New J. Phys.* **2018**, *20*, No. 043008.

(19) Li, Z.; Zeng, Y.; Zhang, J.; Zhou, M.; Wu, W. Observation of negative longitudinal magnetoresistance in the type-II Dirac semimetal $PtSe_2$. *Phys. Rev. B: Condens. Matter Mater. Phys.* **2018**, *98*, 165441.

(20) Mao, H.-K.; Chen, X.-J.; Ding, Y.; Li, B.; Wang, L. Solids, liquids, and gases under high pressure. *Rev. Mod. Phys.* **2018**, *90*, No. 015007.

(21) Gao, C.; Li, R.; Zhong, M.; Wang, R.; Wang, M.; Lin, C.; Huang, L.; Cheng, Y.; Huang, W. Stability and Phase Transition of Metastable Black Arsenic under High Pressure. *J. Phys. Chem. Lett.* **2020**, *11*, 93−98.

(22) Pawbake, A.; Bellin, C.; Paulatto, L.; Béneut, K.; Biscaras, J.; Narayana, C.; Late, D. J.; Shukla, A. Pressure-Induced Phase Transitions in Germanium Telluride: Raman Signatures of Anharmonicity and Oxidation. *Phys. Rev. Lett.* **2019**, *122*, 145701.

(23) O'Neal, K. R.; Cherian, J. G.; Zak, A.; Tenne, R.; Liu, Z.; Musfeldt, J. L. High Pressure Vibrational Properties of WS_2 Nanotubes. *Nano Lett.* **2016**, *16*, 993−999.

(24) Liu, G.; Yu, Z.; Liu, H.; Redfern, S. A. T.; Feng, X.; Li, X.; Yuan, Y.; Yang, K.; Hirao, N.; Kawaguchi, S. I.; Li, X.; Wang, L.; Ma, Y. Unexpected Semimetallic BiS_2 at High Pressure and High Temperature. *J. Phys. Chem. Lett.* **2018**, *9*, 5785−5791.

(25) Sereika, R.; Park, C.; Kenney-Benson, C.; Bandaru, S.; English, N. J.; Yin, Q.; Lei, H.; Chen, N.; Sun, C.-J.; Heald, S. M.; Ren, J.; Chang, J.; Ding, Y.; Mao, H.-k. Novel Superstructure-Phase Two-Dimensional Material 1T-VSe_2 at High Pressure. *J. Phys. Chem. Lett.* **2020**, *11*, 380−386.

(26) Yan, M.; Wang, E.; Zhou, X.; Zhang, G.; Zhang, H.; Zhang, K.; Yao, W.; Lu, N.; Yang, S.; Wu, S.; Yoshikawa, T.; Miyamoto, K.; Okuda, T.; Wu, Y.; Yu, P.; Duan, W.; Zhou, S. High quality atomically thin $PtSe_2$ films grown by molecular beam epitaxy. *2D Mater.* **2017**, *4*, No. 045015.

(27) Pawar, M. S.; Late, D. J. Temperature-dependent Raman spectroscopy and sensor applications of $PtSe_2$ nanosheets synthesized by wet chemistry. *Beilstein J. Nanotechnol.* **2019**, *10*, 467−474.

(28) An, C.; Chen, X.; Zhou, Y.; Zhou, Y.; Zhang, B.; Chen, C.; Yuan, Y.; Zhang, R.; Zhang, L.; Zhu, X.; Yang, Z. Structural, vibrational and electrical properties of type-II Dirac semimetal $PtSe_2$ under high pressure. *J. Phys.: Condens. Matter* **2019**, *31*, 415402.

(29) Shi, J.; Huan, Y.; Hong, M.; Xu, R.; Yang, P.; Zhang, Z.; Zou, X.; Zhang, Y. Chemical Vapor Deposition Grown Large-Scale Atomically Thin Platinum Diselenide with Semimetal-Semiconductor Transition. *ACS Nano* **2019**, *13*, 8442−8451.

(30) Zhao, Y.; Qiao, J.; Yu, P.; Hu, Z.; Lin, Z.; Lau, S. P.; Liu, Z.; Ji, W.; Chai, Y. Extraordinarily Strong Interlayer Interaction in 2D Layered PtS_2. *Adv. Mater.* **2016**, *28*, 2399−2407.

(31) Bhatt, S. V.; Deshpande, M. P.; Sathe, V.; Rao, R.; Chaki, S. H. Raman spectroscopic investigations on transition-metal dichalcogenides MX_2(M = Mo, W; X = S, Se) at high pressures and low temperature. *J. Raman Spectrosc.* **2014**, *45*, 971−979.

(32) Yuan, Y.-F.; Zhang, Z.-T.; Wang, W.-K.; Zhou, Y.-H.; Chen, X.-L.; An, C.; Zhang, R.-R.; Zhou, Y.; Gu, C.-C.; Li, L.; Li, X.-J.; Yang, Z.-R. Pressure-induced enhancement of optoelectronic properties in PtS_2. *Chin. Phys. B* **2018**, *27*, No. 066201.

(33) Wang, Z.; Wu, H. H.; Li, Q.; Besenbacher, F.; Li, Y.; Zeng, X. C.; Dong, M. Reversing Interfacial Catalysis of Ambipolar WSe_2 Single Crystal. *Adv. Sci.* **2020**, *7*, 1901382.

(34) Mao, H. K.; Xu, J.; Bell, P. M. Calibration of the ruby pressure gauge to 800 kbar under quasi-hydrostatic conditions. *J. Geophys. Res.* **1986**, *91*, 4673−4676.

(35) Wang, Y.; Lv, J.; Zhu, L.; Ma, Y. Crystal structure prediction via particle-swarm optimization. *Phys. Rev. B: Condens. Matter Mater. Phys.* **2010**, *82*, No. 094116.

(36) Wang, Y.; Lv, J.; Zhu, L.; Ma, Y. CALYPSO: A method for crystal structure prediction. *Comput. Phys. Commun.* **2012**, *183*, 2063−2070.

(37) Gao, B.; Gao, P.; Lu, S.; Lv, J.; Wang, Y.; Ma, Y. Interface structure prediction via CALYPSO method. *Sci. Bull.* **2019**, *64*, 301−309.

(38) Jain, A.; Ong, S. P.; Hautier, G.; Chen, W.; Richards, W. D.; Dacek, S.; Cholia, S.; Gunter, D.; Skinner, D.; Ceder, G.; Persson, K. A. Commentary: The Materials Project: A materials genome approach to accelerating materials innovation. *APL Mater.* **2013**, *1*, No. 011002.

(39) Kohn, W.; Sham, L. J. Self-Consistent Equations Including Exchange and Correlation Effects. *Phys. Rev.* **1965**, *140*, A1133−A1138.

(40) Perdew, J. P.; Chevary, J. A.; Vosko, S. H.; Jackson, K. A.; Pederson, M. R.; Singh, D. J.; Fiolhais, C. Atoms, molecules, solids, and surfaces: Applications of the generalized gradient approximation for exchange and correlation. *Phys. Rev. B: Condens. Matter Mater. Phys.* **1992**, *46*, 6671−6687.

(41) Kresse, G.; Furthmüller, J. Efficient iterative schemes for ab initio total-energy calculations using a plane-wave basis set. *Phys. Rev. B: Condens. Matter Mater. Phys.* **1996**, *54*, 11169−11186.

(42) Blöchl, P. E. Projector augmented-wave method. *Phys. Rev. B: Condens. Matter Mater. Phys.* **1994**, *50*, 17953−17979.

(43) Wang, Y.; Wang, J. J.; Wang, W. Y.; Mei, Z. G.; Shang, S. L.; Chen, L. Q.; Liu, Z. K. A mixed-space approach to first-principles calculations of phonon frequencies for polar materials. *J. Phys.: Condens. Matter* **2010**, *22*, 202201.

(44) Togo, A.; Oba, F.; Tanaka, I. First-principles calculations of the ferroelastic transition between rutile-type and $CaCl_2$-type SiO_2 at high pressures. *Phys. Rev. B: Condens. Matter Mater. Phys.* **2008**, *78*, 134106.

(45) Wang, Y.; Cong, C.; Qiu, C.; Yu, T. Raman Spectroscopy Study of Lattice Vibration and Crystallographic Orientation of Monolayer MoS_2 under Uniaxial Strain. *Small* **2013**, *9*, 2857−2861.

https://dx.doi.org/10.1021/acs.jpclett.0c01813
J. Phys. Chem. Lett. 2020, 11, 7342−7349